ACS Photonics

pubs.acs.org/journal/apchd5
Letter

Spatiotemporal Exciton Tracking with a SPAD Camera

Diana Dall'Aglio, Guillermo D. Brinatti Vazquez,* Luca Bolzonello, Iris Cusini, Robin Camphausen, and Niek F. van Hulst*

Cite This: ACS Photonics 2025, 12, 1291−1299

Read Online

ACCESS | Metrics & More | Article Recommendations | Supporting Information

ABSTRACT: Spatiotemporal microscopy plays an important role in the quest for highly efficient light harvesting materials as it allows direct tracking of the nanoscale transport of excitons, the carriers of the photon energy. Unfortunately, achieving high resolution in both space and time often requires scanning beam spots or delay lines, limiting these techniques to specialized research groups. To overcome this problem, we introduce a novel implementation of photoluminescence-detected exciton tracking using a camera composed of an array of single-photon avalanche diodes (SPADs), gated with ∼150 ps temporal accuracy. The use of such a SPAD camera drastically simplifies the experiment, is free of moving parts, and provides at least 1 order of magnitude increase in photon collection efficiency due to the parallel multipixel acquisition. Moreover, the camera allows one to implement different super-resolution excitation strategies. Here we show both point and structured excitation in the same device by simply changing the optical element. The structured illumination allows direct retrieval of the diffusion from a single time-resolved imaging without fitting, even at fluences far below exciton−exciton annihilation conditions. We tested the SPAD camera effectiveness by studying the exciton diffusion properties of the organic photovoltaic material PM6, where we measured an exciton diffusion length of 45 nm. Certainly our new implementation, boosted by rapid advances in SPAD technology, will extend the range of both users and applications of spatiotemporal microscopy.

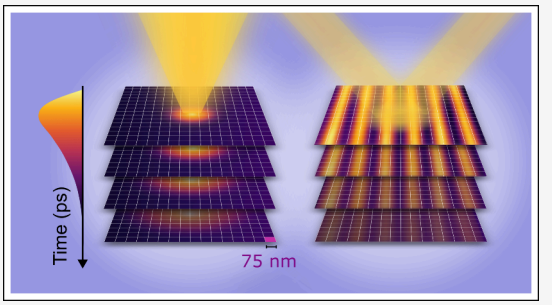

KEYWORDS: *SPAD camera, spatiotemporal microscopy, exciton diffusion, diffusion length, exciton−exciton annihilation, PM6*

INTRODUCTION

Photovoltaic technologies play a crucial role in addressing energy scarcity and the global climate crisis. Among many technologies, organic photovoltaic materials (OPVs) hold significant promise for improving global solar energy production due to their low cost, light weight, and flexible nature. Recent advancements, particularly with nonfullerene acceptors, have led to power conversion efficiencies as high as 19.7%,[1] making them competitive with silicon-based solar cells. For these materials, and many others (perovskites, quantum dots, etc.), understanding and optimizing the nanoscale transport of excitons is crucial to pushing efficiencies closer to their theoretical limits, since it would then be possible to control their movement and thus limit losses. To achieve this, it is essential to track the dynamics of excitons with high spatial and temporal resolutions. This represents an extremely challenging task, as exciton dynamics occur across nanometer length scales and picosecond time scales.[2,3]

A recently introduced group of techniques, usually referred to as spatiotemporal microscopy (SPTM), allows this highly demanding tracking by combining ultrafast spectroscopy techniques together with state-of-the-art microscopy setups.[4−7] SPTM permits the noncontact study of out-of-equilibrium transport phenomena by providing combined spatial (down to nanometers) and temporal (in the femtosecond scale) resolution. These techniques can provide relevant insights into fundamental physical and chemical processes that are usually related to energy dynamics or relaxation. For these reasons, SPTM have lately proven to be extremely useful in tracking photogenerated energy transport in perovskites,[8−11] organic semiconductors,[3,12−14] and 2D materials.[15−17] However, typical methods of SPTM rely on complex setups, with scanning diffraction limited spots and/or delay lines, which are time-consuming to build and demanding to use and maintain, reducing their application to specialized research groups.

One of the main flavors of SPTM is photoluminescence (PL) detected SPTM.[12,18] This technique relies on time-correlated single-photon counting (TCSPC) to retrieve the temporal dynamics of the sample, which is studied in a modified confocal microscopy setup. First, a laser beam is focused to the diffraction limit in the sample using a high numerical aperture (NA) microscope objective to produce the excitation. Then, the photoluminescence is collected and focused on top of a pinhole (sometimes the single-photon

Received: November 26, 2024
Revised: February 10, 2025
Accepted: February 10, 2025
Published: February 17, 2025

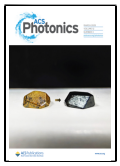

https://doi.org/10.1021/acsphotonics.4c02359
ACS Photonics 2025, 12, 1291−1299

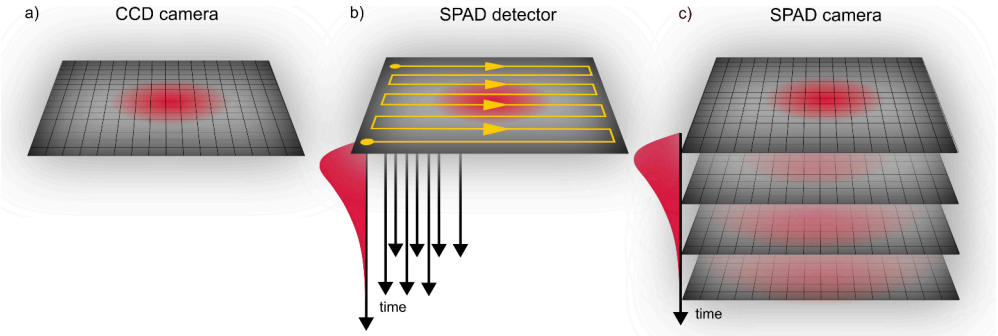

Figure 1. Different optical detection techniques to perform spatiotemporal tracking. (a) A conventional CCD camera allows for parallel acquisition, having a pixelated detector, but its time resolution is limited to the μs range. (b) The high temporal resolution of a SPAD detector can be exploited by spatial scanning and sequential acquisition of TCSPC traces. (c) A SPAD camera combines the respective advantages of a CCD camera and a SPAD by means of an array of single-photon detectors, each of which is able to follow the time evolution of the corresponding spot at the sample.

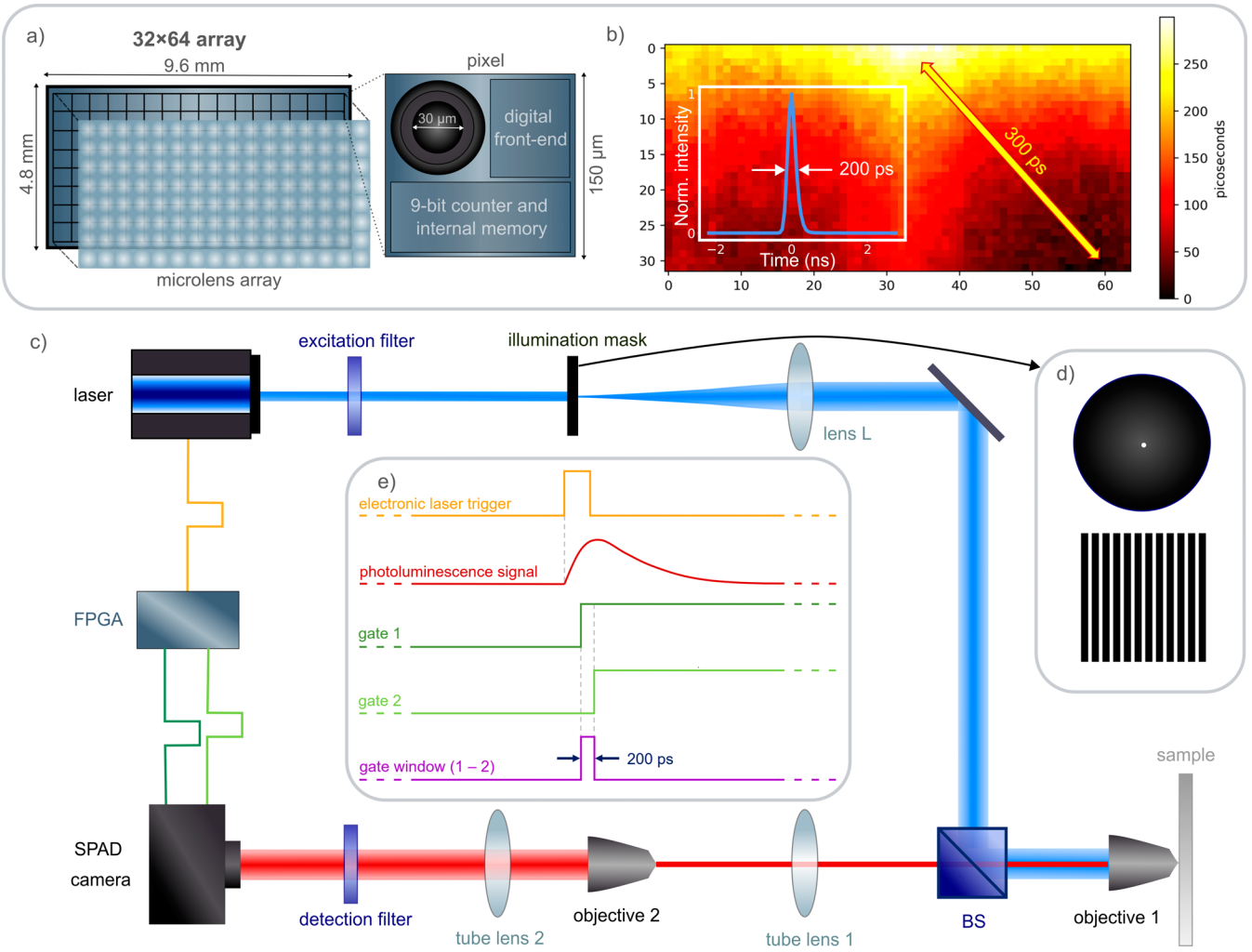

Figure 2. SPAD camera and experimental setup. (a) Structure of the camera chip and structure of each pixel. (b) Camera impulse response function in time and interpixel skew prior to calibration. Inset: instrument response function after calibration, defining the time resolution of the method. (c) Optical microscopy setup: a wide-field fluorescence microscope with the possibility of inserting a transmission mask of choice in the excitation path (blue) and the incorporation of a telescope in the detection path (red) to achieve the required 2000x magnification. (d) Possible illumination masks to be inserted in the excitation path: pinhole (top) and metallic grating (bottom). (e) Scheme of the different pulses and signals in the detection setup, with relative position to one another and qualitative duration.

detector itself) to collect the PL arising from a small spatial region of the sample. Subsequently, unlike what happens in scanning confocal microscopy, the pinhole is transversely scanned in order to obtain a 1D or 2D image of the fixed excitation spot. The spatiotemporal dynamics of the excitation are then retrieved by sequentially acquiring TCSPC traces at each pinhole position (as illustrated in Figure 1b), leading to a serial, time-consuming, and photon inefficient process.

https://doi.org/10.1021/acsphotonics.4c02359
ACS Photonics 2025, 12, 1291−1299

Intensified charge coupled device (ICCD) cameras are an interesting alternative to allow widefield PL detected SPTM. Exciton diffusion in a perovskite thin film was observed using an ICCD.[19] However, the camera intensifier gate-time of around 1 ns constrains the method to species with long lifetimes in the several nanoseconds regime, which is insufficient for many materials, such as OPVs.

Here, to overcome such limitations, we present a novel method of PL detected SPTM to directly and rapidly measure exciton diffusion using a single-photon avalanche diode (SPAD) camera.[20,21] This recently introduced type of camera combines the parallel, multipixel acquisition of CCD cameras (which have slow acquisition speed, as shown in Figure 1a) with the fast, single-photon response of the SPAD detectors in a single device, as represented in Figure 1c. Although the technology is still maturing, many imaging applications have found great advantages in exploiting the features of SPAD arrays. One of the most relevant examples is fluorescence lifetime imaging microscopy (FLIM), where the fast temporal response of the camera excels at the retrieval of lifetime images in a widefield fashion,[22−27] eliminating the need of complex and expensive beam-scanning optics and devices. The single-photon sensitivity of the arrays was also exploited when combined with laser scanning setups to achieve super resolution in confocal[28,29] and multiphoton[30] microscopes, and was also used to enhance single molecule localization[31] and tracking[32] applications. The ability of detecting single photons is also fundamental to quantum imaging applications, where SPAD cameras were extensively investigated.[33−37]

To achieve the required temporal resolution, these SPAD array cameras implement a single-photon counting protocol, either with a time-gating technique (which consists of enabling the SPAD only for a narrow time window) or with a more sophisticated TCSPC system (time-tagging of the detected photons). The latter has a higher collection efficiency, since the detectors are always active, but usually at the expense of the fill-factor, which is reduced due to the more complex pixel architecture and results in a lower photon detection efficiency. More details on these techniques can be found in the cited sources.[21,38,39] Our camera model has a time-gating system, as will be discussed in the Method section.

For SPTM experiments, our SPAD camera allows achieving high spatial resolution on the nanometer scale and temporal resolution down to hundreds of picoseconds (an order of magnitude increase compared to ICCD camera approaches[19]), which is critical for observing fast exciton dynamics. Several key advantages should be noted: the use of a pixelated detector allows the experimental setup to be strongly simplified, as it eliminates the need for scanning optics as well as the data acquisition and analysis. Free of moving parts, the setup is robust to environmental fluctuations and misalignment, ensuring accurate and reliable data collection under varying conditions. Second, the parallel acquisition for all pixels increases the measurement speed and efficiency by up to 2 orders of magnitude (compared to previous works[12,18]). Finally, the camera offers great versatility, as it allows integrating different super-resolution strategies in the same setup with ease, as we will prove by combining diffraction-limited point excitation with the recently introduced structured excitation approach.[13] We describe the main characteristics of the SPAD camera together with the experimental setup in the Method section, followed by the discussion of the results of applying the SPAD camera setup to the study of exciton diffusion in the OPV material PM6.[40−44] This material, also known as PBDB-T-2F, is a p-type polymer electron donor. When combined with nonfullerene electron acceptors Y6[40,45,46] or L8-BO,[44] the resulting binary system exhibits an extremely high current density and power conversion efficiency, resulting in a promising platform for energy applications. Lastly, we highlight some advantages and disadvantages of the use of a SPAD camera for transport applications.

METHOD

The SPAD camera,[47] as shown in Figure 2a, is a multipurpose single-photon counting image sensor that utilizes a 32 × 64 array of 30 μm diameter SPADs arranged in a 150 μm pitch square grid. Each pixel includes the necessary digital electronics for photon counting and features a very low noise level of 100 cps. Additionally, a microlens array optimizes the collection efficiency, achieving a fill factor of up to 80% and high photon detection efficiency in the visible region, with a maximum of about 50% at around 410 nm. Three integrated counters within each pixel can be enabled within a user-defined temporal window (gate signal). By using two gate pulses slightly shifted in time, a time resolution better than 200 ps can be achieved by simply computing the difference between the two counters, effectively isolating the photons detected within the specific time interval defined by the shift. Because each pixel has separate counters, we need to account for variations in the gate pulse arrival time. In Figure 2b, we show the difference in arrival time across the chip, which can be an up to 300 ps delay between the opposite edges. This variation must be corrected to retrieve the full 200 ps time resolution when performing spatiotemporal measurements (Figure 2b, inset).

The optical setup is depicted in Figure 2c. Basically, it can be understood as an inverted wide-field fluorescence microscope, with the only difference being that a transmission mask is placed one focal length away of lens L in the excitation path, which is imaged on the sample. By changing this mask we can easily switch from a diffraction-limited point excitation (using a 20 μm pinhole) to a high frequency sine-like excitation (by using a 20 lines/mm amplitude diffraction grating), as represented in Figure 2d. This allows the achievement of different super-resolution strategies (as we will discuss later) in the same setup and in a very convenient manner.

A high NA (1.4, oil immersion) microscope objective is used both to excite and to collect the photoluminescence from the sample. A 90/10 (T/R) beamsplitter is used to separate the excitation and detection paths instead of the more traditional dichroic mirror in order to achieve high sample (wavelength) flexibility. A microscopy tube lens (Thorlabs TTL200-A) is used to generate an image of the sample on an intermediate plane. Because of the large pixel pitch of the SPAD array, an additional telescope is required to achieve the required magnification. For this purpose, a 10x (Olympus NA 0.25) microscope objective was used together with a 600 mm achromat lens, leading to an overall magnification of 2000x or an equivalent pixel size in the sample of 75 nm. As an illumination source, a supercontinuum laser (NKT Photonics SuperK Extreme) is used. A 5 nm bandpass filter is used to select the desired excitation wavelength. Figure 2e represents the pulse scheme used in the experiment. An electronic trigger pulse is obtained from the laser controller, which is then fed to an adaptive computing board (Red Pitaya, STEMlab 125-14), in charge of generating the two gate pulses. By electronically

https://doi.org/10.1021/acsphotonics.4c02359
ACS Photonics 2025, 12, 1291−1299

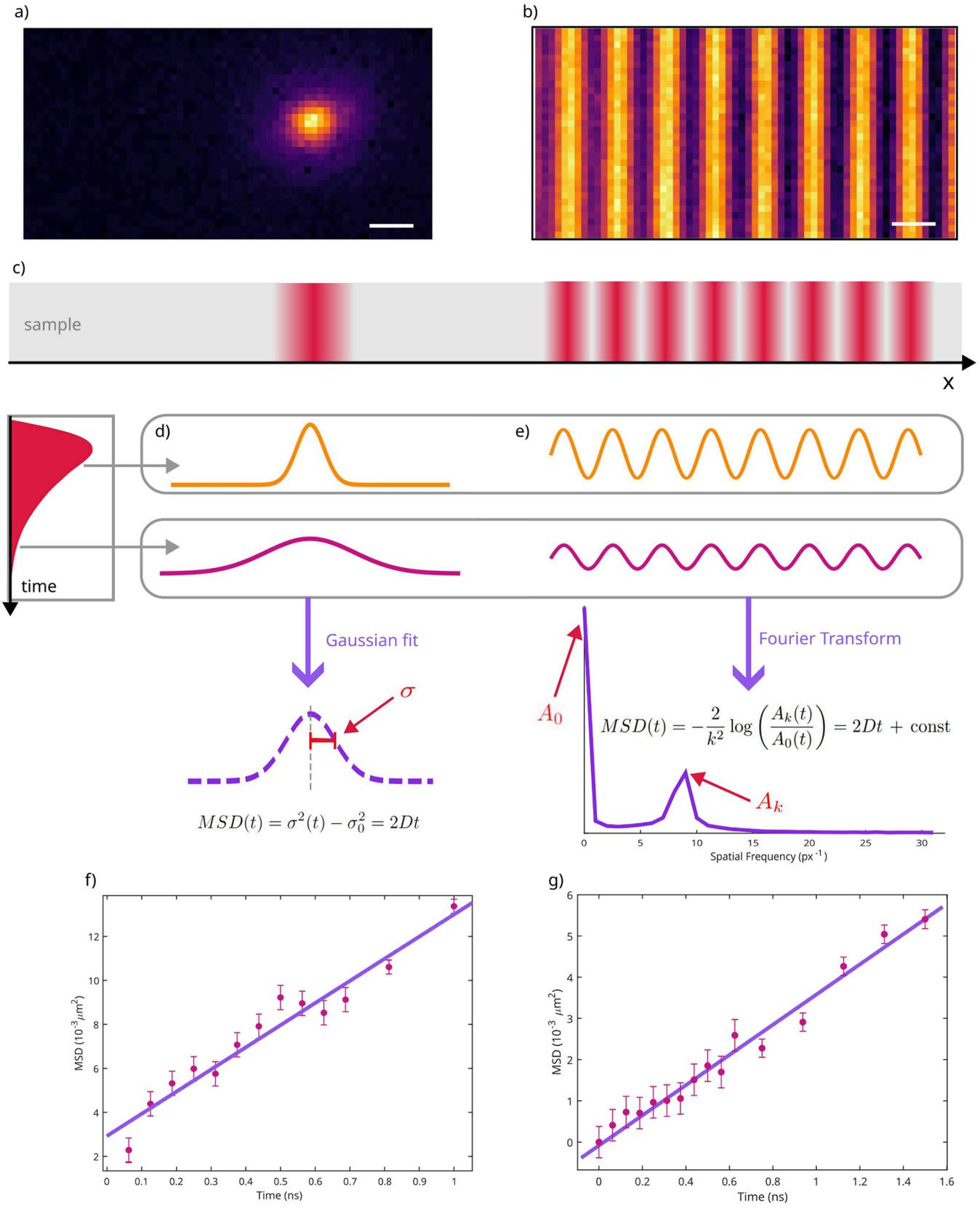

Figure 3. Direct comparison between the two methods of point and structured illumination. (a) Camera view of the photoluminescence spot, obtained with a 20 μm pinhole in the excitation path. (b) Camera view of the periodic illumination pattern generated by the presence of a 20 lines/mm metallic grating as an illumination mask. The scale bars for both (a) and (b) correspond to 500 nm on the sample. (c) Scheme of a sample section, highlighting the distribution of the photoexcitation within the material surface in the two configurations. (d) In the point illumination scheme, the excitation profile can be modeled by a 2D Gaussian curve, which broadens and flattens as time passes: the variation of its standard deviation in time allows to estimate the exciton diffusivity. (e) In the structured illumination method, the excitation profile is a periodic function,

https://doi.org/10.1021/acsphotonics.4c02359
ACS Photonics 2025, 12, 1291−1299

Figure 3. continued

which if Fourier transformed at each time interval gives a diffusivity estimation. (f and g) Linear fits to the MSD data in the point and structured illumination methods, respectively; from the slope one easily extracts the corresponding D value.

scanning these two delay pulses, a full movie can be obtained, showing the spatiotemporal dynamics of our sample. Notice that the camera design circumvents the need for beam-scanning optics, typically required in conventional setups. Instead, it captures spatiotemporal data across the entire region of interest simultaneously, providing a major advantage in speed and greatly simplifying the experimental setup, which is completely free of moving parts.

RESULTS AND DISCUSSION

In Figure 3 we show, side by side, two examples of spatiotemporal microscopy experiments performed in our SPAD array setup. The sample under study is OPV material PM6, which is a p-type polymer electron donor that absorbs and emits in the 500−650 and 700−800 nm wavelength ranges, respectively. First, we focus on point-excitation SPTM, one of the most widely used methods for the direct observation of exciton diffusion.[12−14] As shown in Figure 3a, we start by exciting our OPV material with a diffraction-limited spot. Then, the diffusion properties of the exciton population will result in a broadening compared to the initial width of the excitation, as represented in inset (c). A short video showing the evolution of the photoluminescence signal (for a 600 nJ/cm^2 excitation beam) over sequential time frames is provided as Supplementary Video 1. As this broadening is typically well below the optical resolution limit (diffusion lengths are in the order of few tens of nanometers[6]), the information is recovered by fitting a PSF model, in this case, a 2D Gaussian with a single width parameter σ. This allows one to track the evolution of the width of the exciton population with a resolution just limited by signal-to-noise ratio and thus much better than the optical resolution. As is well-known,[4,7] the mean square displacement (i.e., the measure over time of the deviation of a particle position with respect to a reference point) grows linearly with time at a rate proportional to the diffusivity, which is then easily retrieved by computing a linear fit in a measurement of MSD as a function of time, as shown in Figure 3f.

To achieve these measurements, previous methods[12,18] typically required acquiring TCSPC traces sequentially while scanning the beam over the sample or adjusting the detector position. This approach often results in time-consuming experiments, especially when reconstructing 2D maps, which is why most experiments are limited to single-line scanning, resulting in the loss of information. This leads to a reduced robustness and accuracy on the width determination, as the 1D PSF model used to fit the data has basically the same number of parameters as the 2D model but is evaluated on a much smaller number of data points. Additionally, achieving high spatial resolution requires a small detector (or pinhole) that is at least half the size of the illumination spot on the sample, causing the collection of only a small fraction of the emitted photons, while most are lost. Approaches using cylindrical optics were investigated to partially recover this loss,[48] at the cost of additional experimental complexity and the risk of introducing optical aberrations.

In contrast, using a SPAD array allows for the parallel acquisition of the entire image simultaneously, enabling simple and fast 2D acquisition without a spatial photon loss. For example, the comparison of the SPAD array approach with a 20 × 20 xy scan using a single detector demonstrates a significant efficiency difference: the latter requires 400 individual TCSPC measurements, whereas the time-gated SPAD array only needs measurements equal to the number of time delays of interest, which can be in the order of 10−20. Furthermore, the gating time delay can be set arbitrarily, allowing for efficient time-delay sampling that maximizes diffusion information while minimizing photon loss and experimental duration.[49] An SPTM setup using a SPAD array with integrated TCSPC would fully exploit the PL photons, being limited only by the detection efficiency of each pixel. Although time-gated cameras currently feature larger chips and higher fill factors, TCSPC array cameras are becoming more competitive as the SPAD array technology moves forward.[25]

Opposite to the point-excitation method in Figure 3, we show an alternative implementation of a structured-excitation scheme (StrEET microscopy[13]). As shown in Figure 3b, a sine-like pattern is produced in the sample simply by imaging a diffraction grating. The result of this is a periodic exciton population that reduces its modulation amplitude as the excitons diffuse, as sketched in Figure 3e. The retrieval of the diffusivity is much simpler compared to the point-excitation case as no fitting is required. Instead, a 2D Fourier transform of the data allows us to easily compute the DC and the excitation frequency amplitudes, whose ratio isolates the diffusivity contribution to the amplitude decay. As the excitation is only periodic in the horizontal direction x, all the useful information is found on a single row of our 2D Fourier space (corresponding to $k_y = 0$), as we show in Figure 3e. There, the two peaks required to calculate the MSD (DC and excitation spatial frequencies) are easily distinguished. For more details on how the MSD is calculated, please see ref 13.

As shown in Figure 3g, the diffusivity is again recovered as the slope of the MSD evolution in time. It is important to notice that the use of the SPAD array also greatly simplifies the spatiotemporal experiment in the case of structured excitation. Indeed, the imaging capabilities allow to recover the information simply by taking a 2D Fourier transform of the data, eliminating the need of complex demodulation strategies that require intermediate imaging on a piezo-controlled amplitude mask and the use of complex two-objective configurations, as presented in the single SPAD implementation.[13] It is interesting to notice that, although a single excitation frequency is used for this experiment (as we are investigating an isotropic material), the imaging capabilities of the SPAD camera enable us to explore more complicated excitation structures, such as extending the periodicity also to the vertical direction, allowing the study of nonisotropic diffusion. Moreover, as the Fourier analysis isolates the contribution of each spatial frequency, one can think of using multiple excitation frequencies simultaneously to study nonlinear systems, as it is usually done in transient grating spectroscopy experiments.[50]

https://doi.org/10.1021/acsphotonics.4c02359
ACS Photonics 2025, 12, 1291−1299

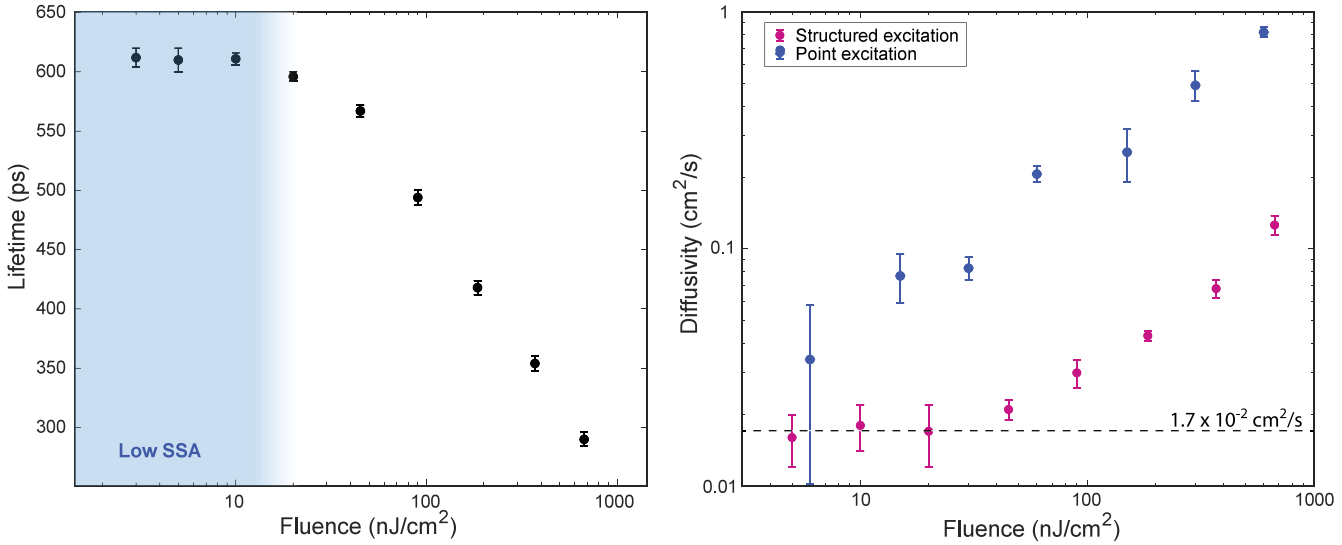

Figure 4. Lifetime (a) and diffusivity (b) measured on PM6 with both point illumination and structured illumination methods.

Imaging also allows one to gather extra information about the sample that is averaged out when using a single detector, such as the presence of structural changes and inhomogeneities. Although the reduced number of pixels in our SPAD array is still small compared to alternatives like ICCD cameras,[19] the less mature SPAD array technology is rapidly developing. Megapixel SPAD arrays performing with lower noise and higher quantum efficiency than the best intensifiers have already been demonstrated.[23,51] Thus, we expect that such cameras with sufficiently high-resolution time-gating or time-stamping will eventually become commercially available. Moreover, the use of a SPAD array with a large number of pixels combined with our structured excitation approach will allow one to easily trace 2D maps of diffusivity by simply reiterating this analysis in few-pixel windows.

In Figure 4 we show a comparison of the performance of the two methods in the determination of the diffusivity constant of a PM6 sample. We start by showing a fluence dependence study of the lifetime of our sample in Figure 4a. This data was obtained from the evolution of the DC component of the structured excitation experiment, as it provides the best signal-to-noise ratio for a given fluence. The lifetime data obtained from the point excitation method (although noisier) shows the same trend and is omitted for simplicity. We can clearly see that the observed lifetime increases with decreasing fluence, stabilizing at a value of τ = 610 ps for fluence values below 10 nJ/cm^2. This effect is well-known and corresponds to a nonlinear contribution to the exciton dynamics due to singlet−singlet annihilation (SSA).[52−54] SSA also affects the diffusion measurements.[12,13,53] For the Gaussian excitation case, this is easily understood as an apparent broadening of the signal due to an increased decay in the center of the excitation spot compared to its tails that is then interpreted as a greater diffusivity. To prevent this kind of artifact, it is important for the measurements to be taken at a sufficiently low fluence, where the effect of SSA becomes negligible.

In Figure 4 we show the fluence dependence of the diffusivity measurements for both methods. Similarly to what is observed for the lifetimes, the values are expected to stabilize at low fluences. We can clearly see this trend for the structured excitation data, showing a diffusivity value of 1.7 × 10^{-2} cm^2/s (or a diffusion length $L_D = \sqrt{2D\tau}$ = 45 nm) and exhibits a stabilizing trend very similar to the lifetime. Our diffusivity value matches previous estimations extracted from the SSA dynamics in a transient absorption spectroscopy (TAS) experiment.[42] Nevertheless, the authors report a much lower diffusion length value as a consequence of a 70 ps lifetime estimation, probably arising from the high fluences required for TAS (usually tens of μJ/cm^2). Different estimations in literature using PL quenching,[42] SSA,[43] and photocurrent measurements[41] lead to different values of diffusivity for PM6 (up to 1 order of magnitude higher than the one reported here). All of these are indirect measurements of the transport properties that require modeling and the estimation of parameters that are hard to measure experimentally (e.g., the exciton capture radius). SPTM techniques are the only ones that achieve direct observation of exciton diffusion, leading to much more accurate results. Additionally, our structured excitation strategy allows us to measure at fluences much lower than previous methods (close to or even below Sun power[13]), guaranteeing an artifact free determination of the diffusivity, as shown in Figure 4b.

For the point-excitation, we see that the apparent diffusivity still decreases for our lowest fluence of 6 nJ/cm^2. From comparing both methods it becomes evident that the threshold fluence for negligible SSA contribution seems to be smaller for the point-illumination experiment, even when the lifetime seems stabilized. To understand this difference, it is important to recall that the relative change in our data due to excitonic transport will improve for a narrower excitation. This is easier to understand in the spatial frequency domain, as the amplitude associated with each spatial frequency k will evolve as $\exp(-k^2Dt)$.[13] Then, higher spatial frequencies decay quadratically faster than lower ones. The faster this decay is, the easier it will overcome the presence of SSA, leading to a reduced nonlinear artifact. Taking a look at our data, we can see that the initial width of the Gaussian corresponds to a value of σ = 247 nm, which corresponds to a cutoff spatial frequency of k_p = 4.05 μm^{-1} compared to k_s = 11.3 μm^{-1} for the grating case, leading to a value of $(k_s/k_p)^2 \simeq 8$, consistent with an SSA threshold roughly 1 order of magnitude higher.

https://doi.org/10.1021/acsphotonics.4c02359
ACS Photonics 2025, 12, 1291−1299

CONCLUSIONS

In this study, we presented a new method for spatiotemporal exciton tracking using a SPAD camera, demonstrating significant improvements in both the speed and simplicity of experimental setups and allowing for measurements with at least 1 order of magnitude higher photon collection efficiency due to the parallel multipixel acquisition. The ability to acquire spatiotemporal data simultaneously across the entire region of interest enables fast and accurate measurement of exciton diffusion. Despite the relatively recent development of SPAD camera technology, our setup has achieved performance comparable to the current state-of-the-art techniques, as demonstrated through our measurements on PM6, where we determined a diffusion length of 45 nm under sufficiently low fluences to minimize nonlinear recombination effects. Moreover, we showed that the inherent flexibility of the camera allows the easy implementation of complementary excitation strategies.

As SPAD camera technology continues to evolve with anticipated improvements in noise performance, time resolution, and pixel density, our method stands to benefit greatly. For instance, a camera with integrated TCSPC in every pixel would maximize the duty cycle, thereby drastically improving the speed and efficiency of the measurements. The absence of moving components allows further miniaturization of spatiotemporal microscopy, and one might even speculate on an integrated optics version. Another exciting future development would be the capability to generate diffusivity maps, which will become feasible as larger sensor arrays are developed. We are convinced that this first application shown here will play an important role in advancing high-efficiency photovoltaic technologies and exploring nanoscale energy transport.

ASSOCIATED CONTENT

Supporting Information

The Supporting Information is available free of charge at https://pubs.acs.org/doi/10.1021/acsphotonics.4c02359.

Time evolution of the PL signal for the point excitation method at a fluence of 600 nJ/cm^2 (video) (MP4)

AUTHOR INFORMATION

Corresponding Authors

Guillermo D. Brinatti Vazquez − *ICFO-Institut de Ciencies Fotoniques, The Barcelona Institute of Science and Technology, 08860 Castelldefels (Barcelona), Spain;* orcid.org/0000-0003-1921-8029; Email: Guillermo.Brinatti@icfo.eu

Niek F. van Hulst − *ICFO-Institut de Ciencies Fotoniques, The Barcelona Institute of Science and Technology, 08860 Castelldefels (Barcelona), Spain; ICREA-Institució Catalana de Recerca i Estudis Avancats, Barcelona 08010, Spain;* orcid.org/0000-0003-4630-1776; Email: Niek.vanHulst@icfo.eu

Authors

Diana Dall'Aglio − *ICFO-Institut de Ciencies Fotoniques, The Barcelona Institute of Science and Technology, 08860 Castelldefels (Barcelona), Spain*

Luca Bolzonello − *ICFO-Institut de Ciencies Fotoniques, The Barcelona Institute of Science and Technology, 08860 Castelldefels (Barcelona), Spain;* orcid.org/0000-0003-0893-5743

Iris Cusini − *ICFO-Institut de Ciencies Fotoniques, The Barcelona Institute of Science and Technology, 08860 Castelldefels (Barcelona), Spain*

Robin Camphausen − *ICFO-Institut de Ciencies Fotoniques, The Barcelona Institute of Science and Technology, 08860 Castelldefels (Barcelona), Spain*

Complete contact information is available at: https://pubs.acs.org/10.1021/acsphotonics.4c02359

Funding

G.D.B.V., L.B., and N.F.v.H. acknowledge support through the MCIN/AEI Projects PID2021-123814OB-I00 and TED2021-129241BI00, the "Severo Ochoa" program for Centres of Excellence in R&D CEX2019-000910-S, Fundacio Privada Cellex, Fundacio Privada Mir-Puig, and the Generalitat de Catalunya through the CERCA program. N.F.v.H. acknowledges the financial support from the European Commission (ERC Advanced Grant 101054846-FastTrack). R.C. acknowledges funding from the European Union's Horizon Europe Research and Innovation Program under Grant 101082596 (QUDICE). This work is part of the ICFO Clean Planet Program supported by Fundació Joan Ribas Araquistain (FJRA).

Notes

The authors declare no competing financial interest.

ACKNOWLEDGMENTS

We thank Francisco Bernal-Texca and Jordi Martorell (ICFO) for the PM6 samples. We thank Micro Photon Devices S.R.L. for providing SPAD camera technical support. D.D. acknowledges QUARMEN Erasmus Mundus Joint Master for the support and the opportunity to conduct her thesis project at ICFO.

REFERENCES

(1) Liu, K.; Jiang, Y.; Ran, G.; Liu, F.; Zhang, W.; Zhu, X. 19.7% efficiency binary organic solar cells achieved by selective core fluorination of nonfullerene electron acceptors. *Joule* **2024**, *8*, 835−851.

(2) Mikhnenko, O. V.; Blom, P. W.; Nguyen, T.-Q. Exciton diffusion in organic semiconductors. *Energy Environ. Sci.* **2015**, *8*, 1867−1888.

(3) Firdaus, Y.; Le Corre, V. M.; Karuthedath, S.; Liu, W.; Markina, A.; Huang, W.; Chattopadhyay, S.; Nahid, M. M.; Nugraha, M. I.; Lin, Y.; et al. Long-range exciton diffusion in molecular non-fullerene acceptors. *Nat. Commun.* **2020**, *11*, 5220.

(4) Ruzicka, B. A.; Werake, L. K.; Samassekou, H.; Zhao, H. Ambipolar diffusion of photoexcited carriers in bulk GaAs. *Appl. Phys. Lett.* **2010**, *97*, 262119.

(5) Wan, Y.; Guo, Z.; Zhu, T.; Yan, S.; Johnson, J.; Huang, L. Cooperative singlet and triplet exciton transport in tetracene crystals visualized by ultrafast microscopy. *Nature Chem.* **2015**, *7*, 785−792.

(6) Ginsberg, N. S.; Tisdale, W. A. Spatially Resolved Photogenerated Exciton and Charge Transport in Emerging Semiconductors. *Annu. Rev. Phys. Chem.* **2020**, *71*, 1−30.

(7) Vazquez, G. D. B.; Morganti, G. L. G.; Block, A.; van Hulst, N. F.; Liebel, M.; Tielrooij, K.-J. Spatiotemporal Microscopy: Shining Light on Transport Phenomena. *Advanced Electronic Materials* **2024**, *10*, 2300584.

(8) Xiao, X.; Wu, M.; Ni, Z.; Xu, S.; Chen, S.; Hu, J.; Rudd, P. N.; You, W.; Huang, J. Ultrafast Exciton Transport with a Long Diffusion Length in Layered Perovskites with Organic Cation Functionalization. *Adv. Mater.* **2020**, *32*, 2004080.

(9) Seitz, M.; Meléndez, M.; Alcázar-Cano, N.; Congreve, D. N.; Delgado-Buscalioni, R.; Prins, F. Mapping the Trap-State Landscape in 2D Metal-Halide Perovskites Using Transient Photoluminescence Microscopy. Advanced. *Opt. Mater.* **2021**, *9*, 2001875.
(10) Seitz, M.; Magdaleno, A. J.; Alcázar-Cano, N.; Meléndez, M.; Lubbers, T. J.; Walraven, S. W.; Pakdel, S.; Prada, E.; Delgado-Buscalioni, R.; Prins, F. Exciton diffusion in two-dimensional metal-halide perovskites. *Nat. Commun.* **2020**, *11*, 2035.
(11) Delor, M.; Weaver, H. L.; Yu, Q.; Ginsberg, N. S. Imaging material functionality through three-dimensional nanoscale tracking of energy flow. *Nature materials* **2020**, *19*, 56−62.
(12) Lo Gerfo M, G.; Bolzonello, L.; Bernal-Texca, F.; Martorell, J.; van Hulst, N. F. Spatiotemporal Mapping Uncouples Exciton Diffusion from SingletSinglet Annihilation in the Electron Acceptor Y6. *J. Phys. Chem. Lett.* **2023**, *14*, 1999−2005.
(13) Brinatti Vazquez, G. D.; Lo Gerfo Morganti, G.; Vasilev, C.; Hunter, C. N.; van Hulst, N. F. Structured Excitation Energy Transfer: Tracking Exciton Diffusion below Sunlight Intensity. *ACS Photonics* **2024**, *11*, 1318−1326.
(14) Berghuis, A. M.; Raziman, T. V.; Halpin, A.; Wang, S.; Curto, A. G.; Rivas, J. G. Effective Negative Diffusion of Singlet Excitons in Organic Semiconductors. The. *J. Phys. Chem. Lett.* **2021**, *12*, 1360−1366.
(15) Lin, Y.; Ling, X.; Yu, L.; Huang, S.; Hsu, A. L.; Lee, Y. H.; Kong, J.; Dresselhaus, M. S.; Palacios, T. Dielectric screening of excitons and trions in single-layer MoS2. *Nano Lett.* **2014**, *14*, 5569−5576.
(16) Ceballos, F.; Bellus, M. Z.; Chiu, H.-Y.; Zhao, H. Probing charge transfer excitons in a MoSe2-WS2 van der Waals heterostructure. *Nanoscale* **2015**, *7*, 17523−17528.
(17) Goodman, A.; Lien, D.-H.; Ahn, G.; Spiegel, L.; Amani, M.; Willard, A.; Javey, A.; Tisdale, W. Substrate-dependent exciton diffusion and annihilation in chemically treated MoS2 and WS2. *J. Phys. Chem. C* **2020**, *124*, 12175−12184.
(18) Akselrod, G. M.; Deotare, P. B.; Thompson, N. J.; Lee, J.; Tisdale, W. A.; Baldo, M. A.; Menon, V. M.; Bulović, V. Visualization of exciton transport in ordered and disordered molecular solids. *Nat. Commun.* **2014**, *5*, 3646.
(19) Li, W.; Huang, M. S. R.; Yadavalli, S. K.; Lizarazo Ferro, J. D.; Zhou, Y.; Zaslavsky, A.; Padture, N. P.; Zia, R. Direct characterization of carrier diffusion in halide-perovskite thin films using transient photoluminescence imaging. *ACS Photonics* **2019**, *6*, 2375−2380.
(20) Rochas, A.; Gosch, M.; Serov, A.; Besse, P.-A.; Popovic, R. S.; Lasser, T.; Rigler, R. First fully integrated 2-D array of single-photon detectors in standard CMOS technology. *IEEE Photonics technology letters* **2003**, *15*, 963−965.
(21) Cusini, I.; Berretta, D.; Conca, E.; Incoronato, A.; Madonini, F.; Maurina, A. A.; Nonne, C.; Riccardo, S.; Villa, F. Historical perspectives, state of art and research trends of SPAD arrays and their applications (Part II: SPAD arrays). *Frontiers in Physics* **2022**, *10*, 906671.
(22) Schwartz, D. E.; Charbon, E.; Shepard, K. L. A single-photon avalanche diode array for fluorescence lifetime imaging microscopy. *IEEE journal of solid-state circuits* **2008**, *43*, 2546−2557.
(23) Morimoto, K.; Ardelean, A.; Wu, M.-L.; Ulku, A. C.; Antolovic, I. M.; Bruschini, C.; Charbon, E. Megapixel time-gated SPAD image sensor for 2D and 3D imaging applications. *Optica* **2020**, *7*, 346−354.
(24) Ulku, A. C.; Bruschini, C.; Antolović, I. M.; Kuo, Y.; Ankri, R.; Weiss, S.; Michalet, X.; Charbon, E. A 512× 512 SPAD image sensor with integrated gating for widefield FLIM. *IEEE J. Sel. Top. Quantum Electron.* **2019**, *25*, 1−12.
(25) Nedbal, J.; Mattioli Della Rocca, F.; Ivanova, I. T.; Allan, A.; Graham, J.; Walker, R.; Henderson, R. K.; Suhling, K. A time-correlated single photon counting SPAD array camera with a bespoke data-processing algorithm for lightsheet fluorescence lifetime imaging (FLIM) and FLIM videos. *Sci. Rep.* **2024**, *14*, 7247.
(26) Castello, M.; Tortarolo, G.; Buttafava, M.; Deguchi, T.; Villa, F.; Koho, S.; Pesce, L.; Oneto, M.; Pelicci, S.; Lanzanó, L.; et al. A robust and versatile platform for image scanning microscopy enabling super-resolution FLIM. *Nat. Methods* **2019**, *16*, 175−178.
(27) Oleksiievets, N.; Mathew, C.; Thiele, J. C.; Gallea, J. I.; Nevskyi, O.; Gregor, I.; Weber, A.; Tsukanov, R.; Enderlein, J. Single-molecule fluorescence lifetime imaging using wide-field and confocal-laser scanning microscopy: A comparative analysis. *Nano Lett.* **2022**, *22*, 6454−6461.
(28) Slenders, E.; Castello, M.; Buttafava, M.; Villa, F.; Tosi, A.; Lanzanò, L.; Koho, S. V.; Vicidomini, G. Confocal-based fluorescence fluctuation spectroscopy with a SPAD array detector. *Light: Science & Applications* **2021**, *10*, 31.
(29) Radmacher, N.; Nevskyi, O.; Gallea, J. I.; Thiele, J. C.; Gregor, I.; Rizzoli, S. O.; Enderlein, J. Doubling the resolution of fluorescence-lifetime single-molecule localization microscopy with image scanning microscopy. *Nat. Photonics* **2024**, *18*, 1059−1066.
(30) Koho, S. V.; Slenders, E.; Tortarolo, G.; Castello, M.; Buttafava, M.; Villa, F.; Tcarenkova, E.; Ameloot, M.; Bianchini, P.; Sheppard, C. J.; et al. Two-photon image-scanning microscopy with SPAD array and blind image reconstruction. *Biomedical Optics Express* **2020**, *11*, 2905−2924.
(31) Slenders, E.; Vicidomini, G. MISM-FLUX: MINFLUX with an array detector. *Physical Review Research* **2023**, *5*, 023033.
(32) Bucci, A.; Tortarolo, G.; Held, M. O.; Bega, L.; Perego, E.; Castagnetti, F.; Bozzoni, I.; Slenders, E.; Vicidomini, G. 4D Single-particle tracking with asynchronous read-out single-photon avalanche diode array detector. *Nat. Commun.* **2024**, *15*, 6188.
(33) Lubin, G.; Tenne, R.; Michel Antolovic, I.; Charbon, E.; Bruschini, C.; Oron, D. Quantum correlation measurement with single photon avalanche diode arrays. *Opt. Express* **2019**, *27*, 32863−32882.
(34) Camphausen, R.; Cuevas, Á.; Duempelmann, L.; Terborg, R. A.; Wajs, E.; Tisa, S.; Ruggeri, A.; Cusini, I.; Steinlechner, F.; Pruneri, V. A quantum-enhanced wide-field phase imager. *Science Advances* **2021**, *7*, eabj2155.
(35) Camphausen, R.; Sansa Perna, A.; Cuevas, Á.; Demuth, A.; Arrés Chillón, J.; Gräfe, M.; Steinlechner, F.; Pruneri, V. Fast quantum-enhanced imaging with visible-wavelength entangled photons. *Opt. Express* **2023**, *31*, 6039−6050.
(36) Severini, F.; Cusini, I.; Madonini, F.; Brescia, D.; Camphausen, R.; Cuevas, Á.; Tisa, S.; Villa, F. Spatially resolved event-driven 24× 24 pixels SPAD imager with 100% duty cycle for low optical power quantum entanglement detection. *IEEE Journal of Solid-State Circuits* **2023**, *58*, 2278−2287.
(37) Madonini, F.; Severini, F.; Zappa, F.; Villa, F. Single photon avalanche diode arrays for quantum imaging and microscopy. *Advanced Quantum Technologies* **2021**, *4*, 2100005.
(38) Bruschini, C.; Homulle, H.; Antolovic, I. M.; Burri, S.; Charbon, E. Single-photon avalanche diode imagers in biophotonics: review and outlook. *Light: Science & Applications* **2019**, *8*, 87.
(39) Becker, W. *Advanced Time-Correlated Single Photon Counting Techniques*; Castleman, A. W., Toennies, J., Zinth, W., Eds.; Springer Berlin Heidelberg: Berlin, Heidelberg, 2005; pp 11−25.
(40) Shoaee, S.; Luong, H. M.; Song, J.; Zou, Y.; Nguyen, T.-Q.; Neher, D. What We have Learnt from PM6:Y6. *Adv. Mater.* **2024**, *36*, 2302005.
(41) Jiang, K.; Zhang, J.; Peng, Z.; Lin, F.; Wu, S.; Li, Z.; Chen, Y.; Yan, H.; Ade, H.; Zhu, Z.; Jen, A. K. Pseudo-bilayer architecture enables high-performance organic solar cells with enhanced exciton diffusion length. *Nat. Commun.* **2021**, *12*, 468.
(42) Sun, F.; Zheng, X.; Hu, T.; Wu, J.; Wan, M.; Xiao, Y.; Cong, T.; Li, Y.; Xiao, B.; Shan, J.; Wang, E.; Wang, X.; Yang, R. 1,5-Diiodocyclooctane: a cyclane solvent additive that can extend the exciton diffusion length in thick film organic solar cells. *Energy Environ. Sci.* **2024**, *17*, 1916−1930.
(43) Xue, P.; Calascibetta, A. M.; Chen, K.; Thorn, K. E.; Jiang, Y.; Shi, J.; Jia, B.; Li, M.; Xin, J.; Cai, G.; Yang, R.; Lu, H.; Mattiello, S.; Liu, Y.; Tang, Z.; Ma, W.; Lu, X.; Meng, Q.; Hodgkiss, J. M.; Beverina, L.; et al. Enhancing exciton diffusion by reducing energy

https://doi.org/10.1021/acsphotonics.4c02359
ACS Photonics 2025, 12, 1291−1299

disorder in organic solar cells. *J. Mater. Chem. A* **2022**, *10*, 24073−24083.
(44) Bernal-Texca, F.; Martorell, J. Four-Terminal Tandem Based on a PM6:L8-BO Transparent Solar Cell and a 7 nm Ag Layer Intermediate Electrode. *Solar RRL* **2024**, *8*, 2300728.
(45) Bolzonello, L.; Bernal-Texca, F.; Gerling, L. G.; Ockova, J.; Collini, E.; Martorell, J.; van Hulst, N. F. Photocurrent-Detected 2D Electronic Spectroscopy Reveals Ultrafast Hole Transfer in Operating PM6/Y6 Organic Solar Cells. *J. Phys. Chem. Lett.* **2021**, *12*, 3983−3988.
(46) Yuan, J.; Zhang, Y.; Zhou, L.; Zhang, G.; Yip, H.-L.; Lau, T.-K.; Lu, X.; Zhu, C.; Peng, H.; Johnson, P. A.; Leclerc, M.; Cao, Y.; Ulanski, J.; Li, Y.; Zou, Y. Single-Junction Organic Solar Cell with over 15% Efficiency Using Fused-Ring Acceptor with Electron-Deficient Core. *Joule* **2019**, *3*, 1140−1151.
(47) Bronzi, D.; Villa, F.; Tisa, S.; Tosi, A.; Zappa, F.; Durini, D.; Weyers, S.; Brockherde, W. 100 000 frames/s 64× 32 single-photon detector array for 2-D imaging and 3-D ranging. *IEEE J. Sel. Top. Quantum Electron.* **2014**, *20*, 354−364.
(48) Magdaleno, A. J.; Cutler, M. M.; Suurmond, J. J.; Meléndez, M.; Delgado-Buscalioni, R.; Seitz, M.; Prins, F. Boosting the efficiency of transient photoluminescence microscopy using cylindrical lenses. *Nanoscale* **2023**, *15*, 14831−14836.
(49) Bolzonello, L.; van Hulst, N. F.; Jakobsson, A. Fisher information for smart sampling in time-domain spectroscopy. *J. Chem. Phys.* **2024**, *160*, 214110.
(50) Huberman, S.; Duncan, R. A.; Chen, K.; Song, B.; Chiloyan, V.; Ding, Z.; Maznev, A. A.; Chen, G.; Nelson, K. A. Observation of second sound in graphite at temperatures above 100 K. *Science* **2019**, *364*, 375−379.
(51) Morimoto, K.; Iwata, J.; Shinohara, M.; Sekine, H.; Abdelghafar, A.; Tsuchiya, H.; Kuroda, Y.; Tojima, K.; Endo, W.; Maehashi, Y.; Ota, Y.; Sasago, T.; Maekawa, S.; Hikosaka, S.; Kanou, T.; Kato, A.; Tezuka, T.; Yoshizaki, S.; Ogawa, T.; Uehira, K.; et al. 3.2 Megapixel 3D-Stacked Charge Focusing SPAD for Low-Light Imaging and Depth Sensing. *IEEE International Electron Devices Meeting (IEDM)*. **2021**, 20.2.1−20.2.4.
(52) Engel, E.; Leo, K.; Hoffmann, M. Ultrafast relaxation and exciton-exciton annihilation in PTCDA thin films at high excitation densities. *Chem. Phys.* **2006**, *325*, 170−177.
(53) Tamai, Y.; Ohkita, H.; Benten, H.; Ito, S. Exciton diffusion in conjugated polymers: from fundamental understanding to improvement in photovoltaic conversion efficiency. *journal of physical chemistry letters* **2015**, *6*, 3417−3428.
(54) Kulig, M.; Zipfel, J.; Nagler, P.; Blanter, S.; Schüller, C.; Korn, T.; Paradiso, N.; Glazov, M. M.; Chernikov, A. Exciton diffusion and halo effects in monolayer semiconductors. *Physical review letters* **2018**, *120*, 207401.

https://doi.org/10.1021/acsphotonics.4c02359
ACS Photonics 2025, 12, 1291−1299